Fast Compressive Sensing Based on Dominant Frequency Estimation

***Abstract*—This work investigates the theoretical analysis to enable fast and accurate estimation of dominant frequencies from randomly sampled signals by compressive sensing (CS). We show that dominant frequencies can be discovered using partially computed Discrete Cosine Transform (DCT). We also propose a new system structure with an estimation unit that enables the signal reconstruction to be selectively bypassed for CS-based devices on signals with dominant frequencies, thus increasing the responsiveness and further reducing the power consumption. For verification, we design a photoplethysmagram (PPG) based heart rate monitor. Our two-step algorithm consists of prior estimation, which extracts the dominant frequency as the heart rate without reconstructing the original signal, and optional sparse reconstruction using Compressive Sensing Matching Pursuit (CoSaMP). The accuracy is tested using MIMIC database. The detected heart rate is within 1 beat per minute from the reference over 99% of the data.**

***Index Terms*—Compressed sensing, Frequency estimation, Discrete cosine transforms, Matching pursuit algorithms, Photoplethysmography**

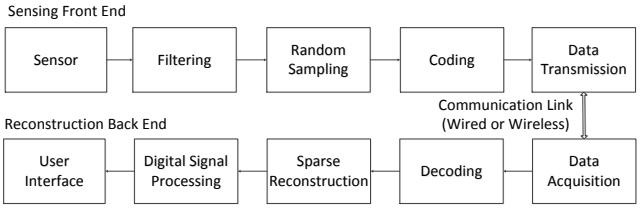

Fig. 1: Traditional CS structure

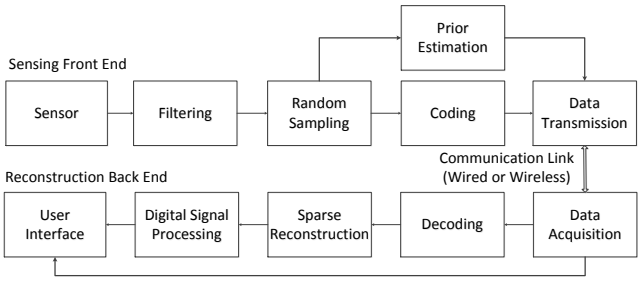

Fig. 2: Proposed CS structure

I. Introduction

Energy consumption has always been a key issue for long-time miniature sensing systems and sensor networks. Low-power design not only helps increase the operation time but also reduce the overall system size since the battery tends to be the largest component in such systems. Compressive sensing (CS) provides a potential solution to this problem. The classic CS approach is to first randomly sample a signal at a low rate and then perform sparse reconstruction to approximate the original by either basis pursuit (BP) [8], i.e. convex optimization, or matching pursuit (MP) [30]. Some CS systems can work even at a sub-Nyqvist rate. However, the potentially complex reconstruction process can increase the system's response time and power consumption by more than can be saved in sampling.

In this work, we explore the inherent signal characteristic to address this problem. One of the most fruitful areas of CS is reconstruction with *known support*, also called *prior knowledge*, which can generally reduce the complexity of CS. In particular, many signals in the natural world possess strong periodic components. In frequency domain, these periodicities appear as one or multiple large coefficients of Discrete Fourier Transform (DFT) or Discrete Cosine Transform (DCT). We introduce a new *frequency-dominant model* to better represent these signals. On top of this model, we show that dominant frequencies can be discovered using partially computed DCT. We also propose a novel system structure with a prior estimation unit as shown in Fig. 2. This unit enables signal reconstruction to be bypassed in some applications, thus increasing the system responsiveness and further reducing the power consumption.

For verification purpose, we design a Photoplethysmogram (PPG)-based heart-rate monitor (HRM). PPG is the collection of vital signs from pulse oximetry, where a single infrared LED or a pair of infrared and red LEDs emit light into body tissues, and one or multiple photo receivers measure the transmittance or reflectance of the light to estimate the absorbance due to the pulsatile arterial blood. PPG monitors are commonly seen in intensive care, elderly care, sports and fitness, newborn screening, and other medical applications. In particular, PPG-based HRM have become popular, because they are more comfortable to wear than the traditional Electrocardiography (ECG)-based HRM. A commercial pulse oximeter consumes 55-120 mW, most of which is consumed by the LEDs [29]. CS can directly save the LED power by reducing the LED on-time, thus making it a natural candidate. We propose a two-step algorithm consisting of prior estimation and Compressive Sensing Matching Pursuit (CoSaMP) [24]. It estimates prior information without actually reconstructing the original signal, thereby enabling accurate heart rate estimation. Our algorithm requires no extra sampling and is of low complexity. Test results on PPG data from MIMIC Database [16] shows that our algorithm accurately reports the heart rate and reconstructs the signal with much fewer iterations than previous works.

This paper first provides a background on CS, DCT, and pulse oximetry. We then formally define the signal model

followed by the dominant frequency estimation algorithm and proof of its probability of success. We present experimental results for designing a PPG based HRM with a discussion of the implications.

II. Background And Related Works

A. Compressive Sensing

A discrete time-frequency signal of N samples can be represented as

$$T = D^{-1}(N)X$$

where T is the time-domain samples, X is the DFT coefficient and $D^{-1}(N)$ is the inverse DCT matrix. A randomly sampled signal with k samples can be represented as

$$PT = PD^{-1}(N)X$$

The matrix P, shown as follows, takes the k random rows out of T.

$$P = \begin{vmatrix} 0 & \dots & 0 & 1 & 0 & \dots & & \\ 0 & \dots & & & 0 & 1 & 0 & \dots \\ & & \dots & & \dots & & & \\ \dots & 0 & 1 & 0 & & \dots & & \end{vmatrix}$$

Let $b = PT$ and $\Phi = PD^{-1}(N)$. Then

$$b = \Phi X$$

where b is the time-domain observation, and X is the frequency-domain signal that we want to recover from b. To differentiate, we call P the *time-domain selection matrix* and Φ the *sampling matrix*. Φ consists of k random rows from the inverse DCT matrix $D^{-1}(N)$.

When $k < N$, this linear system is *underdetermined*, i.e., having infinite solutions. However, if we know X is sparse, then we can search for the most sparse solution out of all the possible combinations of coefficients. The classic CS theory states that an exact reconstruction for a sparse signal is possible from partial knowledge of its Fourier coefficients [8]. An *s-sparse* discrete signal can be reconstructed from $O(s \cdot \log N)$ random samples in time domain with probability $\geq 1 - O(N^{-C})$, where C is a given accuracy parameter and N the size of DFT basis. The actually sparse reconstruction can be solved by BP [8] (l_1-norm) minimization or MP [30]. In practice, this idea can be extended to different transform bases such as wavelet or some redundant basis [9].

Many CS applications have been developed over the past decade [7], [18], [23], [29]. The typical diagram of a CS-based sensing system is shown in Fig. 1. Both the coding unit and decoding unit are optional. The economy of CS is acquired either from transmission link or the sensing unit. For transmission link, CS is used more as a compression than sampling method. A real-time ECG monitor based on CS [18] does uniform sampling but uses a sensing matrix during compression to reduce the bandwidth requirement. Compared with ECG, the sampling process of PPG signal is more expensive due to LED usage as discussed in Section I.

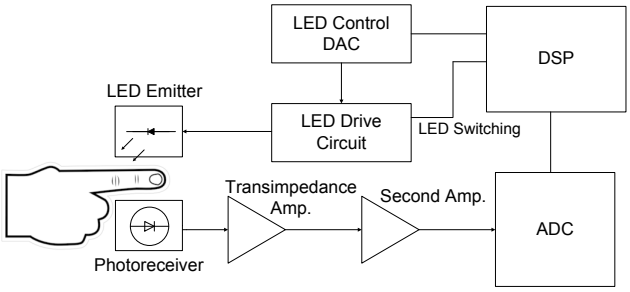

Fig. 3: Pulse oximeter block diagram

How to fast and accurately reconstruct the original signal is very well studied in the CS community. It is generally believed that BP-based algorithms yield higher accuracy if the signal is sufficiently sparse [22], while MP-based greedy algorithms only guarantee to recover an *s-sparse* signal when the number of measurements is proportion to s [30]. On the other hand, the complexity of MP-based algorithms can be only $O(sNk)$ while that of BP is generally much higher [30]. For our application, we choose MP, because we are targeting low-power embedded platforms that usually do not possess the resource to perform convex optimization.

Several previous works attempted to recover PPG signal from compressed samples. The Gradient Projection based Sparse Reconstruction (GPSR) [14] is used in [5], [7]. GPSR is based on convex optimization, which is generally of higher complexity than MP-based greedy algorithms. OMP is used in [6]. A significant drawback of OMP is that it picks only one coefficient every iteration. This inevitably increases the number of iterations and requires a higher order of computational resources. It is estimated that OMP would take tens to even hundreds of iterations for PPG reconstruction [6].

We believe in thoroughly exploring the properties of the source signal before applying the algorithm. Any reconstruction method within the CS framework should not be used as a black box. In our example, the reconstruction is based on CoSaMP [24]. Different from OMP, CoSaMP can rapidly reconstruct the signal by adding multiple coefficients into the support. We customize several parameters based on the characteristics of PPG signals to further reduce the number of iterations.

B. Photoplethysmogram

Photoplethysmogram uses pulse oximetry to measure the absorbance of light due to the pulsatile arterial blood. The system structure of a typical transmittance-type pulse oximeter is shown in Fig. 3. The DSP finds the best signal to noise ratio (SNR) by controlling the LED driver and both amplifiers based on the voltage level of both amplified and raw inputs from the photoreceiver. Heart rate and oxygen concentration (SpO2) are the two most basic indices that can be extracted from PPG. Among several signal-processing techniques used, *weighted moving average* (WMA) [26] is a beat-by-beat algorithm that detects signal peaks in a PPG signal and computes the average

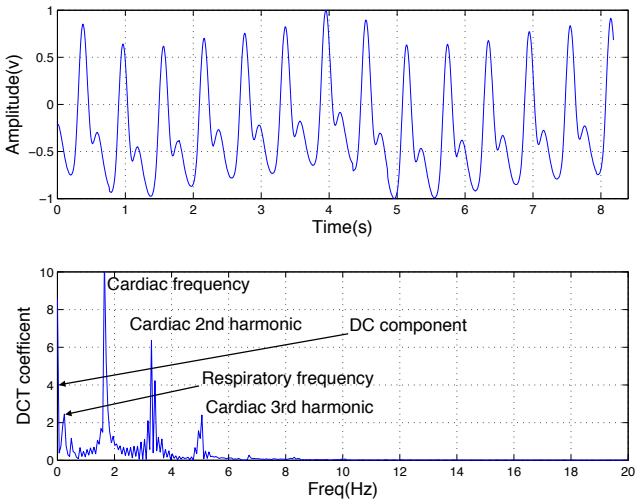

Fig. 4: Typical PPG signal and its DCT transform. Top: PPG signal from patient No. 55 in MIMIC database, bottom: absolute value of the DCT coefficients

HR and SpO2. In practice, SpO2 can be estimated as

$$\text{Ratio} = \frac{AC(\text{Red})}{DC(\text{Red})} \Big/ \frac{AC(\text{IR})}{DC(\text{IR})}$$
$$\text{SpO2} = -2.5\text{Ratio} + 110$$

DFT and DCT are also shown as alternative measures [26]–[28]. In contrast to WMA, these are known as transform-based algorithms. They transform a series of time domain samples to a frequency domain signal and perform spectral analysis. A typical PPG signal and the magnitude of DCT coefficients are shown in Fig. 4. HR can be calculated from the highest peak between 0.5-2.5 Hz. The AC and DC components can be calculated from the cardiac line and DC line, respectively.

C. DCT Basis

The performance of sparse reconstruction relies heavily on the transform basis for two reasons. One is that the basis directly decides the sparsity of the signal. The other is that complex computation can sometimes be optimized on certain bases. In this work, we use DCT basis. It is similar to DFT basis but using only real numbers.

$$x_n = \sum_{k=0}^{N-1} \alpha(k) a_k \cos\left[\frac{\pi(2n+1)}{2N}k\right], n \in [0, N-1]$$
$$a_n = \alpha(n) \sum_{k=0}^{N-1} x_k \cos\left[\frac{\pi(2k+1)}{2N}n\right], n \in [0, N-1] \quad (1)$$

In both equations, $\alpha(n)$ is defined as:

$$\alpha(n) = \begin{cases} \sqrt{\frac{1}{N}} & \text{if } n = 0, \\ \sqrt{\frac{2}{N}} & \text{if } n \neq 0 \end{cases} \quad (2)$$

$x = [x_1 x_2 \cdots x_N]^T$ is the time-domain observation, and $a = [a_1 a_2 \cdots a_N]^T$ is the DCT coefficient vector. The following equation transfers an index in N-point DCT into the corresponding frequency. id is the DCT index number, f_s is the sampling rate, and f_t is the frequency.

$$f_t = \frac{f_s \times id}{2N}; \quad (3)$$

For simplicity, we directly use frequency as the DCT index omitting the projection. In previous work, however, wavelet basis is used to represent PPG signals. We favor DCT in the HRM application for the following reasons.

1. DCT coefficients can be computed fast from FFT [11]. FFT algorithm runs in $O(N \lg N)$ time. Many DSPs are equipped with hardware butterfly units [1] to accelerate FFT. A great advantage over wavelet is that only a linear processing step is needed to compute DCT from FFT.
2. The PPG signal in DCT domain is sparse when only few dominant frequencies exist as shown in Fig. 4. Our study also shows that most PPG signals can be represented using around 60 coefficients in the case of 1024-point DCT.
3. The DCT coefficients can be used directly to compute heart rate and SpO2 level. Thus, no extra time-domain processing is required. In previous works [5]–[7], the heart rate and SpO2 are detected by the extra beat-by-beat analysis after the reconstruction, therefore consuming extra power.

III. Theory

A. Dominant Frequency Signal Model

To describe our algorithm, we first start with a formal definition of dominant frequency:

Definition 1. *A frequency f_k is* dominant *to frequency f_k' with degree $M > 0$ if $|a_k| > |a_{k'}|$ and $|a_k - a_{k'}| = M$.*

In real situations, spectral leakage [19] happens due to the windowing effect of DCT. Spectral leakage represents the energy from a non-integer frequency leaked into the adjacent DCT bins. Spectral leakage reduces the dominance degree, as can be seen in Fig. 4. To overcome this influence, we introduce an extra factor of tolerance β into the definition of a dominant frequency over a range.

Definition 2. *Let $f_k \in \{f_{n_1}, f_{n_2}\}$, $\Gamma = \{f_k - \beta, f_k + \beta\}$. Let $\Gamma_{|a|}$ be the set of all absolute values of DCT coefficients within Γ. We say f_k is dominant in $\{f_{n_1}, f_{n_2}\}$ with degree $M > 0$ if the following holds for all $f_{k'} \in \{f_{n_1}, f_{n_2}\} - \Gamma$.*

$$|a_k| = \sup\{\Gamma_{|a|}\}, \qquad |a_k - a_{k'}| \geq M \quad (4)$$

As the above definition shows, a dominant component can be either plus or minus as long as it stands up in the DCT spectral. The advantage of this model is that it very well quantifies the dominance degree of a DCT component. It is also related to the sparse model. We can loosely interpret a sparse signal under our defined model. It is easily shown that if a signal is s-sparse in DCT domain, then it has s dominant frequencies with a certain degree. We can approximate a signal with s dominant frequencies using the s-sparse model by discarding all the coefficients that are not dominant. In

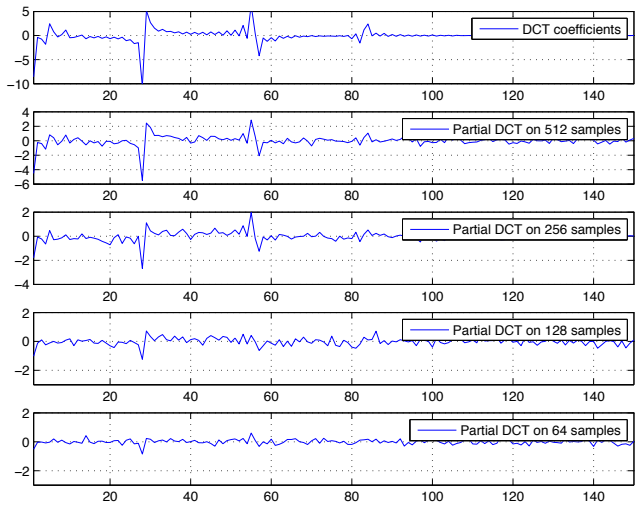

Fig. 5: Partially computed DCT using different number of random samples

fact, it has been shown in [13] that a signal is compressible if the sorted transform coefficients decay exponentially. This is equivalent to exponentially decayed dominance degrees.

B. Dominant Frequency Estimator

We use partially computed DCT transform from random samples to estimate the dominant frequencies defined in Eq. (5).

$$C_{\text{partial}} = DP^T b \tag{5}$$

where D is the DCT matrix, P is the selection matrix, and b is the time-domain sample. Letting Φ^+ denote the pseudo-inverse of the sensing matrix Φ, Eq. (5) is equivalent to

$$C_{\text{partial}} = \Phi^+ b \tag{6}$$

Fig. 5 shows the original DCT and the partially computed DCT with a different number of samples. It is easy to see the high resemblance of the dominant frequencies. If one frequency is dominant enough in the original DCT, it may be still dominant in the partially computed DCT. This method is mentioned in different contexts from the previous works [15], [24], but neither shows that it can be used to directly extract a significant parameter. In this section, we analyze the correctness of this approach. Particularly, we show that it will pick up the dominant frequency with high probability when the dominance degree M is sufficiently large. We first present the following theorem and also provide a sketch of the proof. We assume that the source $\{x_n\}_{0\le n\le N-1}$ is normalized to $[-1,1]$. We define the following notations:

X: $\sum_{i=0}^{N-1} a_i x_i$
Y: $\sum_{i=0}^{N-1} b_i x_i$
$\{x_n\}$: the time-domain samples,
$\{a_n\},\{b_n\}$: the two rows from the DCT matrix, $0 \le n \le N-1$
$\{K_1,\ldots,K_k\}$: a subset of size k randomly taken from $\{0,1,\ldots,N-1\}$ with $k \ll N$
X_K: $\sum_{i=K_1}^{K_k} a_i x_i$
Y_K: $\sum_{i=K_1}^{K_k} b_i x_i$.

Theorem 1. *If $X-Y=M$ for some $M>0$, then*

$$\Pr(X_K > Y_K) \ge \frac{M^2}{\frac{N-K}{N-1}\frac{2N-M^2}{K} + M^2} \tag{7}$$

.

Proof. We define random variable (r.v.) Z to take on $\{(a_n - b_n)x_n\}_{n=0,1,\ldots,N-1}$. We also use the following notations.

$$Var[Z] = \frac{\sigma_Z^2}{N},$$
$$\bar{Z} = \sum_{i=0}^{N-1} (a_i - b_i)x_i,$$
$$Z_K = X_K - Y_K$$

Obviously, $E[X_K] = \frac{K}{N}X$ and $E[Y_K] = \frac{K}{N}Y$. From Chebyshev-Cantelli inequality [17] we have:

$$\Pr(X_K - Y_K > 0) = \Pr(X_K - Y_K - \frac{k}{N}M > -\frac{k}{N}M)$$
$$\ge 1 - \frac{Var[X_K - Y_K]}{Var[X_K - Y_K] + \frac{k^2}{N^2}M^2} \ge \frac{\frac{k^2M^2}{N^2}}{Var[Z_K] + \frac{k^2}{N^2}M^2} \tag{8}$$

We define another r.v. Z' to take on $\{Z_k\}_{k=0,1,\ldots,N-1}$. Z_K is the sum of k samples drawn out of N without replacement. We denote them as $\{Z'_i\}_{i=1,2,\ldots,k}$. We have $Cov(Z'_i, Z'_j)_{i\ne j} = -\frac{\sigma_Z^2}{N-1}$. It follows that

$$Var[Z_K] = Var\left[Z'_1 + \ldots + Z'_k\right] \tag{9}$$
$$= k^2 \frac{N-k}{N-1}\frac{\sigma_Z^2}{k} \tag{10}$$

We need to develop an upper bound for σ_Z^2.

$$\sigma_Z^2 = \sum_{i=0}^{N-1} \frac{[(a_i - b_i)x_i - \bar{Z}]^2}{N}$$
$$= \sum_{i=0}^{N-1} \left[\frac{(a_i - b_i)^2 x_i^2}{N}\right] - 2\bar{Z}\sum_{i=0}^{N-1}\frac{[(a_i - b_i)x_i]}{N} + \bar{Z}^2$$
$$= \sum_{i=0}^{N-1} \frac{[(a_i - b_i)^2 x_i^2]}{N} - \frac{M^2}{N^2} \le \sum_{i=0}^{N-1}\frac{[(a_i - b_i)^2]}{N} - \frac{M^2}{N^2}$$
$$\le \frac{2}{N} - \frac{M^2}{N^2} \tag{11}$$

Here, we use the fact that $x_i \le 1$ and $\bar{Z} = \frac{M}{N}$. Since DCT matrix is orthogonal, $\sum_{i=0}^{N-1} a_i^2 = \sum_{i=0}^{N-1} b_i^2 = 1$ and $\sum_{i=0}^{N-1} a_i b_i =$

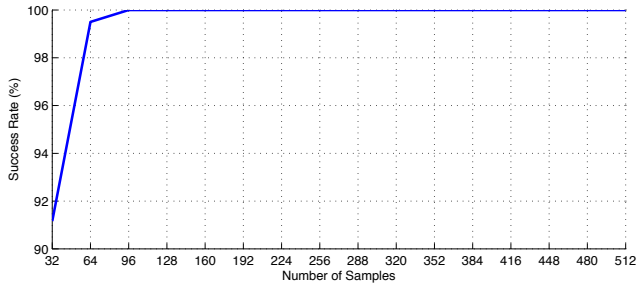

Fig. 6: Success rate of the frequency estimator

0. Substituting σ_Z^2 into Eq. (10) and then into Eq. (8), we have:

$$\Pr(X_K > Y_K) \geq \frac{\frac{k^2M^2}{N^2}}{k^2\frac{N-k}{N-1}\frac{\sigma_Z^2}{k} + \frac{k^2M^2}{N^2}} \tag{12}$$

$$\geq \frac{M^2}{\frac{N-k}{N-1}\frac{2N-M^2}{k} + M^2} \tag{13}$$

□

This problem is actually about two random variables that have a gap between their expectations. We want to find the relationship between them in terms of the gap. The theorem implies that we can extract the dominant frequencies with the maximum of partial DCT coefficients as $X_K = \sum_{i=K_1}^{K_k} a_i x_i$. $x_{K_1}, \ldots, x_{K_k}$ is our time domain observation and $a_{K_1}, \ldots, a_{K_k}$ is the corresponding partial row in DCT matrix. In the example of PPG signal, we use 1024-point DCT and continuously monitored the PPG signal in MIMIC database [16]. When the heart rate is stable, the dominance degree M is over 9. The probability of success is 93.5% for 256 random samples and 85.8% for 128 random samples using Eq. (13) .

This is just a loose bound derived from all the samples at the maximum value in Eq. (11). It is hard to put a tight bound without knowing the distribution of the source signal. However, if we can assume that $Ex[\{x_n\}_{n=0,1,\ldots,N-1}]$ is around 0, then we can approximate $\sum_{i=0}^{N-1}[(a_i-b_i)^2x_i^2]/N$ with $(\sum_{i=0}^{N-1}[x_i^2]/N)(\sum_{i=0}^{N-1}[(a_i-b_i)^2]/N)$. According to Popoviciu's inequality [17] on variances, this would be less than $1/N$. That would give us 96.7% for 256 random samples and 92.6% for 128 samples. The real situation should be much higher. Fig. 6 shows the success rate of 10,000 tests using a 1024-point segment with a dominance degree of 9.8 from patient No. 55 in MIMIC database. The success rate is overwhelmingly high when the number of samples is over 96.

In reality, however, M is unknown. We will next develop an estimator for M and its confidence interval as defined in [17]. Given $\{Z_i'\}_{i=1,2,\ldots,k}$ and $Z_K = X_K - Y_K = M'$, we now consider how closely we can estimate M. It is proved in [17] that we can estimate M using the expectation and variance of Z' for the signal that has a normal distribution.

$$\Pr\left(\frac{\bar{Z}' - \frac{M}{N}}{S/\sqrt{k}} \leq z_{\alpha/2}\right) = 1-\alpha \tag{14}$$

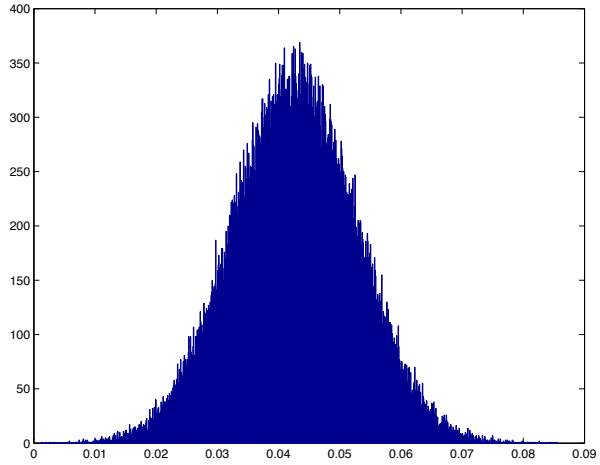

Fig. 7: Distribution of $(\bar{Z}' - M/N)/(S/\sqrt{k})$

Here we use the notation

$$\bar{Z}' = \frac{\sum_{i=1}^{k} Z_i'}{k} = \frac{M'}{k}$$

$$S = \sqrt{\sum_{i=1}^{k} \frac{(Z_i' - \bar{Z}')^2}{k}}$$

$z_{\alpha/2}$ can be derived from the normal distribution $N(0,1)$. For example, $z_{.025} = 1.96$ and $z_{.050} = 1.645$. This can usually be done by a lookup table. Even if the original signal is not normal, $(\bar{Z}' - M/N)/(S/\sqrt{k})$ has an approximate $N(0,1)$ when sample size $k \geq 50$ [17]. Fig. 7 clearly shows this distribution, which is created from 100,000 tests using the data of patient No. 55.

In practice, we can fix α and lower bound of M as M_L. We also put a threshold on M' to decide whether M is large enough. The following has to be satisfied for $M \geq M_L$.

$$M' \geq \frac{M_L k}{N} + \frac{z_{\alpha/2} S k}{\sqrt{k}} \tag{15}$$

For example, if we want $M_L = 5$ with 90% of confidence then we would need $M' > 1.0226$ with $S = 0.0213$ for the data shown in Fig. 4.

C. The Role of Randomness

It is obvious that if all the time-domain samples are zeros or close to zero, then the algorithm will fail, since the samples do not provide enough information to extract the dominant frequency or to reconstruct the signal. The randomness actually ensures that this happens with a very small probability. The variance term in Eq. (15) also adds a correction factor to reduce the chance of false detection.

IV. Design Example

A. Heart Rate Estimation Algorithm

Our heart-rate detection algorithm has two parts: prior estimation and sparse reconstruction. We want to find the greatest peak in the cardiac frequency range of 0.5–2.5 Hz and

the dominance degree of the peak frequency. If it is larger than the threshold, then we are confident that it is the heart rate. If not, we need to reconstruct the original signal for further signal processing. The sparse reconstruction will be discussed in the next section.

A partial DCT transform actually performs dot products of size k for N times. Instead of doing this to the whole DCT basis $D_{N\times N}$, we can pick up the rows in the range $\{\text{R: } 0.5 \text{ Hz} \le f \le 2.5 \text{ Hz}\}$ and store it locally. The algorithm is shown in Algorithm 1. We assume that $Max(C)$ operation finds the maximum absolute value in set C and outputs a 2-tuple (c_{max}, f_{max}) for the DCT coefficient and the corresponding frequency. We use the same notation for error β and Γ as in the Section III-A. An acceptable error range for heart rate is usually ± 1 beat per minute (bpm), $\beta = 1/60$ Hz.

Input: selection matrix P, time domain sample Y, partial DCT matrix D', confidence interval α, error β
Output: heart rate H_{bpm} beats per minute over the sampling period of N
begin
  $C_{partial} \leftarrow D'Y$; /* partial DCT */
  $(c_{max}, f_{max}) \leftarrow Max(C_{partial})$;
  $\Gamma = [f_{max} - \beta, f_{max} + \beta]$;
  for (f, c_f) *in* $\{R - \Gamma\}$ **do**
    $M' \leftarrow |c_{max} - c_f|$;
    $TH_L \leftarrow \frac{Mk}{N} + \frac{z_{\alpha/2} Sk}{\sqrt{k}}$; /* Eq. (15) */
    if $M' < TH_L$ **then**
      $CoSaMP()$;
      $Peak\_Detection()$;
      return;
    end
  end
  $H_{bpm} \leftarrow 60 \times f_{max}$;
  return;
end

Algorithm 1: Heart Rate Detection Algorithm

The actual range of the PPG signal is usually determined by the range of ADC. There is no need for normalization but to adjust the threshold of the dominance level. The running time of the prior estimation part is dominated by variance calculation in Eq. (15), which takes $O(k \cdot c_R)$ time with c_R being the size of R. Since $c_R, k \ll N$, it can be easily implemented on a mobile device or a low-power DSP [1].

B. Sparse Reconstruction

Heart rate variation or significant noise will result in an insufficient dominance degree. The original needs to be reconstructed in order to perform a beat-by-beat analysis. Our intention is not to develop a universal algorithm but one that works effectively for this special type of signal.

We use CoSaMP to reconstruction the signal. The standard CoSaMP algorithm is shown as follows. $Max_n(S)$ finds the best n support from set S. Φ_T denotes the matrix restricted to the columns in set T.

Input: sampling matrix Φ, time domain sample y, sparsity level s, stopping criteria P
Output: s-sparse representation vector x
begin
  $x^0 \leftarrow 0$; /* x_i is the i^{th} approximation */
  $e \leftarrow y$; /* current error */
  $i \leftarrow 1$; /* iteration count */
  while P *not true* **do**
    $C \leftarrow \Phi^+ y$; /* formula (6) */
    $\Omega \leftarrow Max_{2s}(C)$;
    $T \leftarrow \Omega \cup x^{i-1}$;
    $b_T \leftarrow \Phi_T^+ y$; /* least square */
    $x^i \leftarrow Max_s(b)$;
    $r \leftarrow y - \Phi x^i$; /* time domain residue */
    $i \leftarrow i + 1$;
  end
end

Algorithm 2: Basic CoSaMP

Fig. 8 shows the reconstructed signal using 30, 60, and 90 coefficients. The original algorithm does not work well for our application as expected, for two reasons.

1. As mentioned above, CoSaMP also uses partial DCT to approximate the original. It can easily be seen in Fig. 5 that the gap between each pair of frequencies becomes much smaller or even gets reversed. Even if a component is not dominant enough, it can still be wrongly selected into the best $2s$ support. This is especially significant when we do not have an accurate estimate of the sparsity level.
2. The l_2-norm of the time domain residue r is commonly used as a stopping criterion, but it does not correctly reflect the accuracy of the reconstruction as shown in Fig. 8. We also observed that increasing the sparsity level does not always help when the total number of samples is relatively small (below 200) compared to the cardinality of the basis. In Fig. 8, the signal reconstructed with sparsity level of 60 actually generates more error than 30 does, even though the residual l_2-norm is smaller.

We reduce the size of the basis to solve this problem. Fig. 9 shows the histogram of 1024-point DCT coefficients over the PPG data of 55 patients in MIMIC database. Every count in the histogram is weighted by the absolute value of the corresponding coefficient. The majority of the coefficients is concentrated in bins 1–120. To ensure that our algorithm can also work for signals with severe noise, we set up a separate threshold for the frequencies outside the above range. We still pick them up if they are dominant enough. This works much better than just restricting the basis to bins 1–120.

Fig. 10 shows the reconstruction over different sparsity level after reducing the basis. We use the record of patient No. 208 because of its low dominance degree throughout the whole data. As can be seen from Table I, 399 out of 433 segments require reconstruction. We compare the reconstructed signal with the original to compute l_2-norm instead of the residue. This gives us the accuracy but it is not available in the

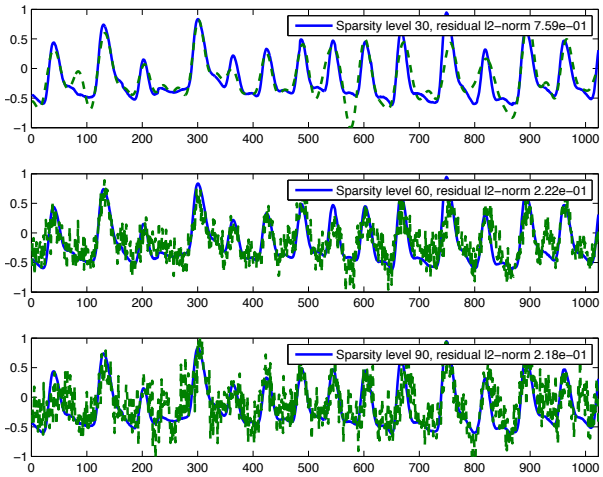

Fig. 8: PPG reconstruction with 192 samples

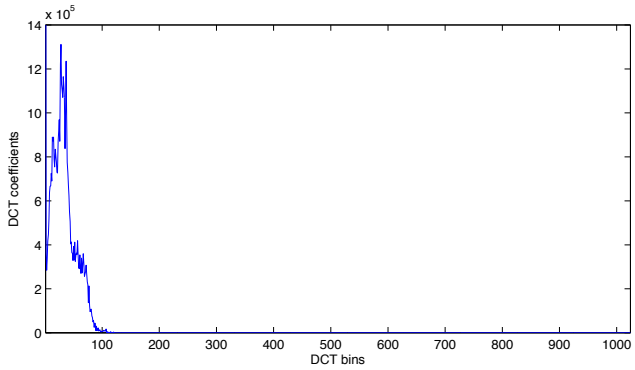

Fig. 9: Weighted histogram of DCT coefficients

real application. It is obvious that adding more support will improve the accuracy, but it will also increase the complexity of the reconstruction. In practice, we find that a support of size around 60 is enough for heart rate detection. The main test result is shown in the next section. Fig. 11 shows the reconstruction of one DCT segment. We could still see the difference that generates large l_2-norm of the time domain signal, but there is no need to add more coefficients to the support for this application.

C. Test Result

1) Detection Rate: We continuously divide the digital samples from MIMIC database into 1024-point segments and run our algorithm on them. The sampling rate is 125 Hz. The number of random samples is 192 over each DCT segment. We find it is very difficult to get a stable performance of the sparse reconstruction when given fewer samples. Some other parameters for the experiment are shown as follows.

a) interval $\alpha = 0.1$ with $z_{\alpha/2} = 1.645$
b) Threshold on dominance degree M_L: 5
c) Threshold out of the range M_R: 4
d) Tolerance β: 1 DCT bin

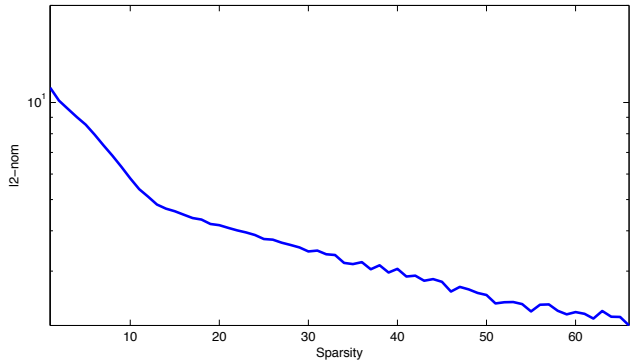

Fig. 10: Reconstruction with different sparsity level. Data from patient No. 208 in MIMIC database. l_2-norm is computed using the original signal.

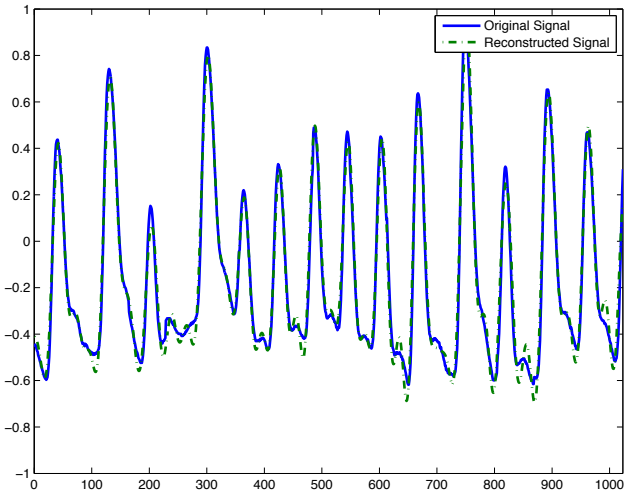

Fig. 11: Reconstruction with the proposed CoSaMP

e) CoSaMP stopping criteria: residual l_2-norm $< 10^{-10}$, or residue l_2-norm difference between current and last iteration $< 10^{-10}$, or iteration count > 100

The main result is shown in Table I. The heart rate on some segments is detected just by prior estimation while others by beat-by-beat analysis after reconstruction. The error columns in the table are average error in the unit of *bpm*. We manually removed some segments severely polluted by noise. Examples of such segments are shown in Fig. 12. The results show that our algorithm is effective to over 99% of the data.

The reference heart rate is calculated by two algorithms, a beat-by-beat peak searching algorithm [10] for the reconstructed signal and a DCT algorithm for the signal with the prior estimation. For the peak searching algorithm, the signal first goes through a band pass filter (BPF). Then each sample is compared with the thresholds for peak detection. Two sets of adaptive threshold are maintained for peaking searching, one for heart beat and the other for noise peaks. For the DCT algorithm, a full DCT is performed to the original signal to compute the heart rate.

TABLE I: Detection rate

Patient #	Seg. Tol.	Det. Rate.	Recons. Tol.	Recons. Err.	Prior Esti. Tol.	Prior Esti. Err.
55	14206	99.58%	5363	0.08	8843	0.25
208	433	95.61%	399	0.30	34	0.76
209	8590	94.99%	8037	0.25	553	0.41
210	5835	95.29%	5326	0.23	509	0.89
211	8866	99.37%	4750	0.05	4116	0.29
212	17570	99.88%	1951	0.09	15619	0.32
216	10107	98.43%	2773	0.28	7334	0.45
218	8792	97.71%	4357	0.19	4435	0.45
219	9638	99.22%	2935	0.10	6703	0.35
220	482	99.99%	190	0.00	292	0.41
221	10087	99.96%	917	0.07	9170	0.28
224	20199	99.68%	4879	0.16	15320	0.28
225	17935	99.64%	6357	0.07	11578	0.34
226	12204	99.56%	2346	0.13	9858	0.29
230	3400	99.94%	1006	0.00	2394	0.28
231	18083	99.89%	15441	0.01	2642	0.27
237	16318	99.53%	4590	0.10	11728	0.34
252	10901	99.75%	2371	0.10	8530	0.30
430	2753	98.80%	1658	0.13	1095	0.30
437	19978	99.26%	5601	0.19	14377	0.27
438	19746	98.27%	18074	0.08	1672	0.56
439	19872	99.82%	2855	0.11	17017	0.24
446	10511	97.47%	9043	0.13	1468	0.19
449	6353	99.98%	1659	0.01	4694	0.53
451	11661	99.81%	4599	0.02	7062	0.29
452	13861	97.35%	10154	0.21	3707	0.28
453	17461	96.08%	14554	0.21	2907	0.46
454	14374	95.11%	11776	0.25	2598	0.53
456	15776	99.32%	6428	0.14	9348	0.27
466	5927	99.95%	1132	0.02	4795	0.33
471	25291	98.66%	10036	0.16	15255	0.37
472	2997	94.56%	2145	0.31	852	0.60
474	3850	99.92%	97	0.14	3753	0.31

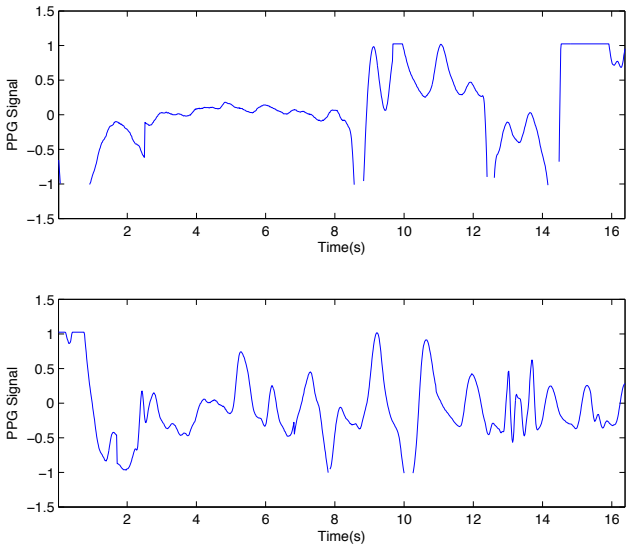

Fig. 12: Corrupted and noisy PPG signal segments. Top: data containing NaN (not a number), bottom: data with high noise

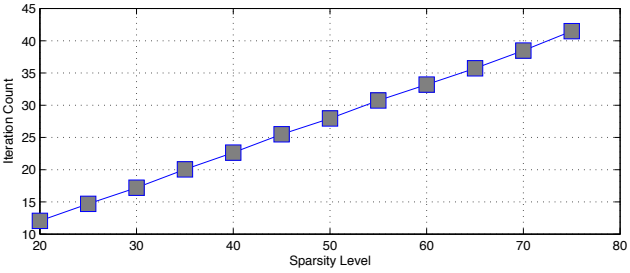

Fig. 13: Iteration count vs. sparsity level

The average iteration count of the reconstruction over different sparsity levels is shown in Fig. 13. Again, the data of patient No. 208 is used. The traditional OMP algorithm would take at least 50% more iterations since the OMP iteration count is roughly the same with the size of support.

2) Power Consumption: The under sampling rate (*USR*) is generally used to quantify the rate of random sampling. It is equal to N/k with the same N and k defined in Section II-A. For our work, the *USR* is around 5. The previous works claim they can reconstruct the PPG signal with a *USR* of under 20 without losing much information [6]. However, the target of our reconstruction algorithm is the data with high level noise and high heart rate variation. The prior estimation stage will naturally screen the signal to avoid reconstruction for the more sparse signal generally shown in other works. We believe the setting of our experiment is closer to the real applications.

The power saving mainly comes from the optional reconstruction in the back end. It is hard to estimate the actual effect without the detailed information. However, as shown in Table I, for PPG signal with a stable heart rate, over 99% of the reconstruction can be saved with very little power increase in the front end. The system response is also greatly improved.

As a justification for the power saving effect of CS, the LED power saved at the *USR* of 5 is around 0.99 mW for the high-end pulse oximeter hardware platform [3] using a low-power DSP TMS320C5515 [1]. This alone is already around 16% of the system power. The PPG samples are taken and processed during the interrupt service routine (ISR) by the DSP. The parameters used for this calculation are shown as follows.

Average ISR time:	600 μs [7]
DSP active power:	59.1 mW@100MHz [2]
DSP standby power:	0.7 mW [2]
IR LED on power:	19.8 mW (60mA at 3.3V)
IR LED on time:	50 μs
Sampling rate:	125 Hz

The system takes 6.32 mW overall before applying CS. Over 50% of the power is actually saved from setting the DSP to standby mode than turning off the LED.

One would think to uniformly sample the signal at 25 Hz and detect the heart rate. We run our peak searching algorithm to the down-sampled data from patient No. 208 and find a maximum heart rate error of over 1.8 *bpm* for the same data set used in Table I. This is much larger than the error after the sparse reconstruction, which is around 0.6 *bpm*. Several heart beat peaks are detected as noise peaks when using down-

sampled signal. Even though the frequency range of interest is 0.4-5 Hz [26] for the PPG signal, detection algorithms require a higher sampling rate to tolerate noise and irregular heart beats. Most of the systems are actually running at high sampling rates of 100-1k Hz [3], [12], [20], [21], [25], [31].

D. Discussion

Increasing the number of random samples inevitably increases the power consumption, but it actually discourages reconstruction since the probability of discovering the dominant cardiac frequency in prior estimation becomes higher. It would be very interesting to find an optimal point for power consumption on a real platform. This will be done for our future work.

For the segments needing reconstruction, we did observe some significant deviation from beat-by-beat analysis as large as 7–10 bpm, but we ascribe that to the environment noise and corrupted samples such as the data shown in Fig. 12. Our implementation of the detection algorithm could not even yield a reliable result under these conditions. The overwhelmingly large number of the total segments still validates the correctness of our algorithm.

For the segments estimated with the prior, the error is mainly caused by the spectral leakage as discussed in Section III-A. One obvious way to deal with the error is to decrease the minimum sampling interval, i.e. shorten the width of each DCT bin. Another is to change the signal to a zero-padded DCT as discussed in [13]. This topic is beyond the scope of this work.

Our sparse reconstruction obviously takes advantage of the low-pass filtering to the source signal, as it makes the source signal sparse. This could be implemented in hardware [4] without significantly increasing the power consumption. The intuition is that the proposed CoSaMP should also be effective on unfiltered data. As our future work, we will acquire unfiltered data using real hardware to confirm the performance of our algorithm.

V. Conclusions

We have presented a novel fast CS system structure based on dominant frequency estimation. The correctness is proved by both statistical analysis and a real implementation of a PPG-based HRM with the heart-rate detection algorithm consisting of prior estimation and sparse reconstruction based on CoSaMP. Experimental results show it promising on real applications. The low complexity of the prior estimation enables implementation on the embedded sensing front end or mobile devices. We also showed that the fast greedy algorithm of CoSaMP to be a viable option, in contrast to traditional BP or OMP used in previous works. We accelerate the process by taking advantage of the dominance frequencies and the sparsity of PPG signals. Our experience shows two important implications: 1) The signal properties should be thoroughly studied in order to reduce the complexity of CS. 2) The sparse reconstruction should be specific to the target application. There is no need to design a universal algorithm that may over- or under-reconstruct the signal.

References

[1] C5000 DSP Info. Page. http://www.ti.com/lsds/ti/dsp/c5000_dsp/overview.page.

[2] Power Consumption Summary for C5000 DSP. http://processors.wiki.ti.com/index.php/TMS320C5504/05/14/15/32/33/34/35_Power_Consumption_Summary.

[3] Pulse Oximeter Implementation on the TMS320C5515 DSP Medical Development Kit. http://www.ti.com/lit/an/sprab37a/sprab37a.pdf.

[4] Wrist based HRM Reference Design. http://www.ti.com/lit/ug/tidu125/tidu125.pdf.

[5] Pawan K. Baheti and H. Garudadri. An ultra low power pulse oximeter sensor based on compressed sensing. In *Wearable and Implantable Body Sensor Networks, 2009. BSN 2009. Sixth International Workshop on*, pages 144–148, June 2009.

[6] Pawan K. Baheti and Harinath Garudadri. Heart rate and blood pressure estimation from compressively sensed photoplethysmograph. ICST, 5 2010.

[7] Pawan K. Baheti, Harinath Garudadri, and Somdeb Majumdar. Blood oxygen estimation from compressively sensed photoplethysmograph. In *Wireless Health 2010*, WH '10, pages 10–14, New York, NY, USA, 2010. ACM.

[8] E.J. Candes, J. Romberg, and T. Tao. Robust uncertainty principles: exact signal reconstruction from highly incomplete frequency information. *Information Theory, IEEE Transactions on*, 52(2):489–509, Feb 2006.

[9] Emmanuel J Candes, Yonina C Eldar, Deanna Needell, and Paige Randall. Compressed sensing with coherent and redundant dictionaries. *Applied and Computational Harmonic Analysis*, 31(1):59–73, 2011.

[10] FC Chang, CK Chang, CC Chiu, SF Hsu, and YD Lin. Variations of hrv analysis in different approaches. In *Computers in Cardiology, 2007*, pages 17–20. IEEE, 2007.

[11] Wen-Hsiung Chen, C. Smith, and S. Fralick. A fast computational algorithm for the discrete cosine transform. *Communications, IEEE Transactions on*, 25(9):1004–1009, Sep 1977.

[12] R Couceiro, P Carvalho, RP Paiva, J Henriques, and J Muehlsteff. Detection of motion artifacts in photoplethysmographic signals based on time and period domain analysis. In *Engineering in Medicine and Biology Society (EMBC), 2012 Annual International Conference of the IEEE*, pages 2603–2606. IEEE, 2012.

[13] Marco F. Duarte and Richard G. Baraniuk. Spectral compressive sensing. *Applied and Computational Harmonic Analysis*, 35(1):111 – 129, 2013.

[14] M.A.T. Figueiredo, R.D. Nowak, and S.J. Wright. Gradient projection for sparse reconstruction: Application to compressed sensing and other inverse problems. *Selected Topics in Signal Processing, IEEE Journal of*, 1(4):586–597, Dec 2007.

[15] A.C. Gilbert, M.J. Strauss, and J.A. Tropp. A tutorial on fast fourier sampling. *Signal Processing Magazine, IEEE*, 25(2):57–66, March 2008.

[16] Ary L. Goldberger, Luis A. N. Amaral, Leon Glass, Jeffrey M. Hausdorff, Plamen Ch. Ivanov, Roger G. Mark, Joseph E. Mietus, George B. Moody, Chung-Kang Peng, and H. Eugene Stanley. Physiobank, physiotoolkit, and physionet: Components of a new research resource for complex physiologic signals. *Circulation*, 101(23):e215–e220, 2000.

[17] R.V. Hogg and E.A. Tanis. *Probability and Statistical Inference*. Number v. 978, nos. 0-58475 in Probability and Statistical Inference. Prentice Hall, 2010.

[18] K. Kanoun, H. Mamaghanian, N. Khaled, and D. Atienza. A real-time compressed sensing-based personal electrocardiogram monitoring system. In *Design, Automation Test in Europe Conference Exhibition (DATE), 2011*, pages 1–6, March 2011.

[19] Steven M. Kay. *Modern spectral estimation : theory and application*. Prentice Hall signal processing series. Prentice Hall, Englewood Cliffs (N.J.), 1988.

[20] Jaywoo Kim, Mi-hee Lee, Hyoung-Ki Lee, Kiwan Choi, SeokWon Bang, and Sangryong Kim. Heart rate monitor for portable mp3 player. In *Engineering in Medicine and Biology Society, 2005. IEEE-EMBS 2005. 27th Annual International Conference of the*, pages 5207–5210. IEEE, 2006.

[21] Rajet Krishnan, Balasubramaniam Natarajan, and Steve Warren. Two-stage approach for detection and reduction of motion artifacts in photoplethysmographic data. *Biomedical Engineering, IEEE Transactions on*, 57(8):1867–1876, 2010.

[22] Stefan Kunis and Holger Rauhut. Random sampling of sparse trigonometric polynomials, ii. orthogonal matching pursuit versus basis pursuit. *Found. Comput. Math.*, 8(6):737–763, November 2008.

[23] M. Lustig, D.L. Donoho, J.M. Santos, and J.M. Pauly. Compressed sensing mri. *Signal Processing Magazine, IEEE*, 25(2):72–82, March 2008.

[24] D. Needell and J. A. Tropp. CoSaMP: Iterative signal recovery from incomplete and inaccurate samples. *ArXiv e-prints*, March 2008.

[25] Sokwoo Rhee, Boo-Ho Yang, and Haruhiko Harry Asada. Artifact-resistant power-efficient design of finger-ring plethysmographic sensors. *Biomedical Engineering, IEEE Transactions on*, 48(7):795–805, 2001.

[26] T.L. Rusch, R. Sankar, and J.E. Scharf. Signal processing methods for pulse oximetry. *Computers in Biology and Medicine*, 26(2):143 – 159, 1996.

[27] J.E. Scharf, S. Athan, and D. Cain. Pulse oximetry through spectral analysis. In *Biomedical Engineering Conference, 1993., Proceedings of the Twelfth Southern*, pages 227–229, 1993.

[28] J.E. Scharf and T.L. Rusch. Optimization of portable pulse oximetry through fourier analysis. In *Biomedical Engineering Conference, 1993., Proceedings of the Twelfth Southern*, pages 233–235, 1993.

[29] M. Tavakoli, L. Turicchia, and R. Sarpeshkar. An ultra-low-power pulse oximeter implemented with an energy-efficient transimpedance amplifier. *Biomedical Circuits and Systems, IEEE Transactions on*, 4(1):27–38, Feb 2010.

[30] J.A. Tropp and A.C. Gilbert. Signal recovery from random measurements via orthogonal matching pursuit. *Information Theory, IEEE Transactions on*, 53(12):4655–4666, Dec 2007.

[31] Zhilin Zhang, Zhouyue Pi, and Benyuan Liu. Troika: A general framework for heart rate monitoring using wrist-type photoplethysmographic signals during intensive physical exercise. *Biomedical Engineering, IEEE Transactions on*, 62(2):522–531, Feb 2015.